

# Novel organic-inorganic layered oxide with spin ladder structure

B. Ingham<sup>1</sup>, J. L. Tallon<sup>1,2</sup>, S. V. Chong<sup>2</sup>, R.-S. Liu<sup>3</sup> and L.-Y. Jang<sup>4</sup>

<sup>1</sup>Victoria University of Wellington, P.O. Box 600, Wellington, New Zealand

<sup>2</sup>Industrial Research Ltd., P.O. Box 31310, Lower Hutt, New Zealand

<sup>3</sup>Department of Chemistry, National Taiwan University, Taipei, Taiwan, ROC and

<sup>4</sup>National Synchrotron Radiation Research Center, Hsinchu, Taiwan, ROC

(Dated: November 14, 2018)

Structural analysis of a layered manganese tungstate diaminoalkane hybrid series suggests that this compound forms a spin- $\frac{5}{2}$  spin-ladder structure. We use X-ray diffraction, electron microscopy and x-ray absorption spectroscopy results to infer the structure. DC magnetization of the manganese compound and a possible copper analogue appear to show that the manganese system behaves like 1-dimensional antiferromagnetic Heisenberg chains (i.e.  $J_{\parallel} \gg J_{\perp}$ ) while the copper system is fitted well by a  $S = \frac{1}{2}$  spin ladder model, giving the parameters  $g = 1.920 \pm 0.008$ ,  $J_{\parallel}/k_B = -0.3 \pm 1.4\text{K}$ ;  $J_{\perp}/k_B = 213.6 \pm 1.1\text{K}$ . The ability to tune adjacent inorganic layers of the hybrid materials by altering the length of the organic ‘spacer’ molecules gives enormous promise for the use of these materials, especially when doped, to provide a greater understanding of spin ladder systems.

PACS numbers: 61.10.Ht, 61.10.Nz, 75.75.+a, 81.07.Pr

## INTRODUCTION

Spin ladders conceptually represent a transition from 1D to 2D magnetism, although they have actually proven to be more complex and exhibit interesting behavior. Since the discovery of spin-ladder cuprates in 1991 [1], there has been much interest in the phenomena observed in these materials. Spin ladders with an even number of ‘legs’ are predicted (and observed) to have a spin gap [2, 3, 4]. The cuprate spin ladder  $\text{SrCuO}_3$ , and its extensions, have been heavily studied because of the potential for superconductivity due to the presence of the spin gap and their structural similarity to the HTS cuprates [4, 5]. Despite this, superconductivity has not yet been observed except in the  $(\text{Sr,Ca})_{14}\text{Cu}_{24}\text{O}_{41}$  system under high pressure [4, 6].

Besides the cuprates, several other systems are also recognized as spin ladder compounds, including  $\text{M}^{2+}\text{V}_2\text{O}_5$  [4, 7, 8],  $(\text{VO})_2\text{P}_2\text{O}_7$  [2, 3, 9], and  $(\text{C}_5\text{H}_{12}\text{N})_2\text{CuBr}_4$  [10, 11].

The vanadate and cuprate systems listed above all have spin  $S = \frac{1}{2}$  ( $\text{V}^{4+}$  and  $\text{Cu}^{2+}$ ). As such, the only calculated models available are for  $S = \frac{1}{2}$  systems [7]. There are a small number of reports of systems with  $S = 1, \frac{3}{2}, 2$  and  $\frac{5}{2}$ ; all of these involve metal-organic complexes with organic ‘rungs’ of the ladders [12, 13, 14, 15, 16]. To the best of our knowledge, no oxide-based spin ladders have been reported with  $S > \frac{1}{2}$ .

Layered organic-inorganic hybrids, based on tungsten oxide layers separated by organic diamines of various lengths comprise a structurally 2-dimensional system where the proximity and hence the coupling of adjacent layers can be controlled, in principle, by the length of the organic intercalates [17, 18, 19]. Recently, we have succeeded in synthesizing layered organic-inorganic hybrid materials that incorporate magnetic transition metal

ions within the inorganic layers [20]. Here we present the structural findings that lead us to believe that these compounds are capable of forming spin ladder-like structures, and present a preliminary study of their magnetic properties.

## EXPERIMENTAL

Manganese tungstate hybrids, (Mn,W)-DAn, were synthesized by dissolving tungstic acid,  $\text{H}_2\text{WO}_4$ , and  $\alpha,\omega$ -diaminoalkanes ( $\text{C}_n$ ,  $n = 2, 6, 8, 12$ ) separately in hot aqueous ammonia solution and then adding together. Nitrogen gas was bubbled at a moderate rate through the stirred solution as a cold aqueous solution of  $\text{MnCl}_4$  was quickly added. A precipitate immediately formed that darkened with time. The excess solvent was evaporated over a water bath. The use of nitrogen gas was essential to prevent the formation of  $\text{MnO}_2$ . The products were filtered and washed with ethanol and dried under vacuum overnight.

A copper tungstate-1,6-diaminohexane hybrid, (Cu,W)-DA6, could not be synthesized in the same way as the (Mn,W)-DAn samples because of the preferential formation of the  $[\text{Cu}(\text{NH}_3)_4]^{2+}$  complex. Instead, copper tungstate hydrate was soaked in a solution of 1,6-diaminohexane dissolved in toluene for several weeks to form the hybrid, which was then filtered and washed with ethanol and dried under vacuum overnight.

XRD powder spectra were obtained using a Philips PW1700 series powder diffractometer employing  $\text{Co K}\alpha$  radiation ( $\lambda = 1.789 \text{ \AA}$ ). Transmission electron microscopy (TEM) images and selected area electron diffraction (SAED) photographs were obtained using a JEOL 2011 high-resolution instrument with a  $\text{LaB}_6$  filament operated at 200 kV. Energy dispersive X-ray analysis (EDX) was performed using a Leo 440 SEM with an

Oxford ISIS EDX system attached. Infrared spectra were obtained using a Bomem DA8 FT spectrometer over the range 450–4000  $\text{cm}^{-1}$  with a resolution of 2  $\text{cm}^{-1}$ , using the KBr pellet method. Several manganese tungstate hybrid samples were sent to the National Synchrotron Radiation Research Center in Taiwan for x-ray absorption near edge spectroscopy (XANES) and extended x-ray absorption fine structure (EXAFS) measurements. Spectra were obtained at both the Mn K-edge and W L3-edge and fitted using the FEFF and FEFFIT analysis programs. DC magnetization measurements were performed using a Quantum Design MPMS XL SQUID magnetometer at applied fields up to 1 T. Powder samples were ground and 5–20 mg tightly sealed in a gelatin capsule with negligible magnetic susceptibility.

### STRUCTURAL DETERMINATION OF (MN,W)-DAN

Ideally, to determine the structure of an unknown material, single crystal x-ray diffraction would be performed on suitably large ( $\gtrsim 100 \mu\text{m}$ ) crystals. However for the organic-inorganic hybrids, the maximum crystal size observed is  $\sim 10 \mu\text{m}$  [20]. As a result, a combination of methods were used to elucidate a structure.

XRD powder spectra are given for the (Mn,W)-DAn series in Figure 1. In each case a series of  $00l$  lines are evident (as marked). This is characteristic of layered structures and the  $d$ -spacing given by the lines corresponds to the interlayer spacing (e.g. references [21, 22, 23]). When compared with the number of carbons,  $n$ , in the alkyl chain, the  $d$ -spacing follows linearly as  $d = 1.05n + 7.893\text{\AA}$ . The C–C bond length in an alkyl chain is 1.54  $\text{\AA}$  and the bond angle is 109.4 $^\circ$ , giving a longitudinal distance per C–C bond of 1.26  $\text{\AA}$ . Comparing this with the slope of 1.05, we conclude that the organic molecules lie at an angle to the organic plane of 56.5 $^\circ$ .

The distance from one layer to the next is  $d = d_{\text{oxide}} + 2d_{\Delta N} + ((n-1)d_{\text{C-C}} + 2d_{\text{N-C}}) \sin \theta$ , where the distances  $d_i$  are as shown in Figure 2. Extrapolating to  $n = 0$  and substituting  $d = 7.893$ ,  $d_{\text{N-C}} = 1.47 \sin(54.7^\circ) = 1.20$ ,  $d_{\text{C-C}} = 1.26$  and  $\theta = 56.4^\circ$ , we obtain  $d_{\text{inorg}} + 2d_{\Delta N} = 6.94\text{\AA}$ .  $d_{\Delta N}$  is expected to be very small (i.e. the nitrogen atoms of the amine groups lying in plane with any apical oxygen atoms) or even slightly negative. Thus from the oxide layer thickness of 6.94  $\text{\AA}$  we conclude there is a bilayer of  $\text{WO}_6$  octahedra joined at their apices, as one  $\text{WO}_6$  octahedron is  $\sim 3.65\text{--}3.9$   $\text{\AA}$  from one apex to the opposing apex [24].

Infrared spectra of the (Mn,W)-DAn hybrid series (Figure 3) exhibit an identical series of lines at low wavenumbers, corresponding to the inorganic modes. Hence the structure of the inorganic layer is the same for all of the hybrids, regardless of the length of the intercalated organic molecule. In addition, there are  $-\text{NH}_2$

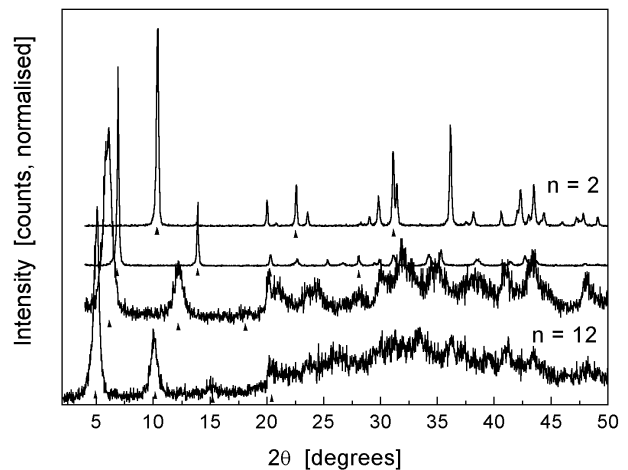


FIG. 1: XRD spectra of the (Mn,W)-DAn hybrids,  $n = 2, 6, 8, 12$  (top to bottom).

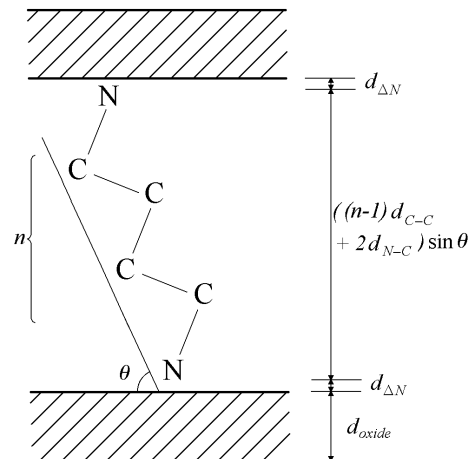


FIG. 2: Schematic diagram of the organic-inorganic hybrid.

modes present and no  $-\text{NH}_3^+$  modes, in contrast with the pure tungsten hybrids ( $\text{WO}_4$ -DAn) [25].

A high-resolution TEM image of (Mn,W)-DA6 is given in Figure 4. Comparing the spacing of the bright spots (corresponding to tungsten atoms) along the two principal axes reveals that the distance between tungsten atoms in the  $b$ -direction is almost exactly double that of the  $a$ -direction. The manganese atoms are thought to lie in the stripes between the tungsten atoms. The doubling in the  $b$ -direction is also evident from SAED photographs (Figure 5), which give  $a = 5.03\text{\AA}$ ,  $b = 10.42\text{\AA}$  ( $\pm 5\%$ );  $b/a = 2.070$  and  $\gamma = 89.7^\circ$ .

From elemental microanalysis combined with EDX we can determine the composition of the hybrids. The results are given in Table I. The metal:tungsten:oxygen ratios are also very close to the inferred stoichiometric values of 1:1:4, even if the molar ratio of the starting materials was varied to  $\text{Mn}_{0.3}\text{W}_{0.7}$ , for instance. No other elements from the starting materials were detected in the

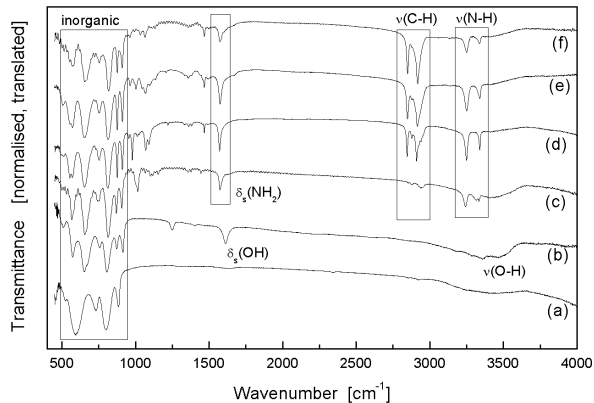


FIG. 3: Infrared spectra of manganese tungstate-based materials: (a)  $\text{MnWO}_4$ ; (b)  $\text{MnWO}_4 \cdot n\text{H}_2\text{O}$ ; (c) (Mn,W)-DA2; (d) (Mn,W)-DA6; (e) (Mn,W)-DA8; (f) (Mn,W)-DA12.

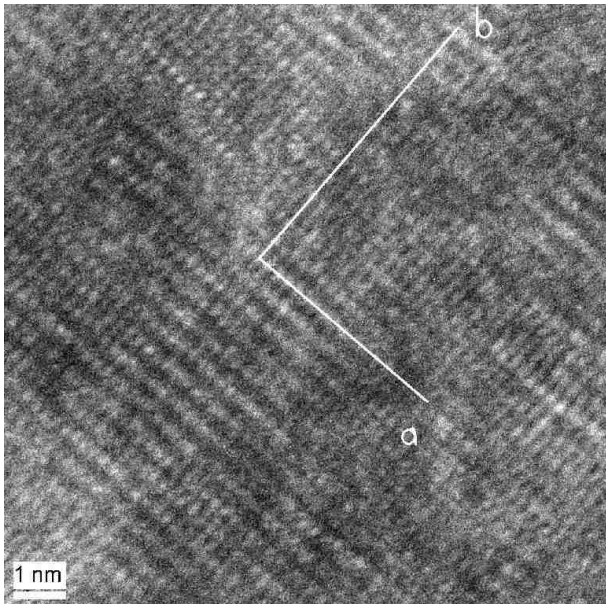


FIG. 4: High-resolution TEM image of (Mn,W)-DA6, with axes indicated.

EDX spectra. The organic ratios are also in good agreement with the expected values: DA2:  $\text{C}_2\text{H}_{8-10}\text{N}_2$ , DA6:  $\text{C}_6\text{H}_{16-18}\text{N}_2$ , DA8:  $\text{C}_8\text{H}_{20-22}\text{N}_2$ , DA12:  $\text{C}_{12}\text{H}_{28-30}\text{N}_2$ . The inorganic:organic ratios are relatively consistent and close to 1:0.5, indicating that for every two  $\text{MnWO}_4$  formula units in the cell, there is one organic molecule. This is consistent with the bilayer found via XRD. The uncertainty in H content arises from its low atomic weight but is pertinent to the question as to whether the organic molecules are terminated by  $-\text{NH}_2$  or  $-\text{NH}_3^+$ . Fortunately, this question is resolved both by the IR spectra and the x-ray absorption data, as discussed next.

XANES at the W L1-edge and the Mn K-edge demonstrated that the manganese tungstate hybrids all have

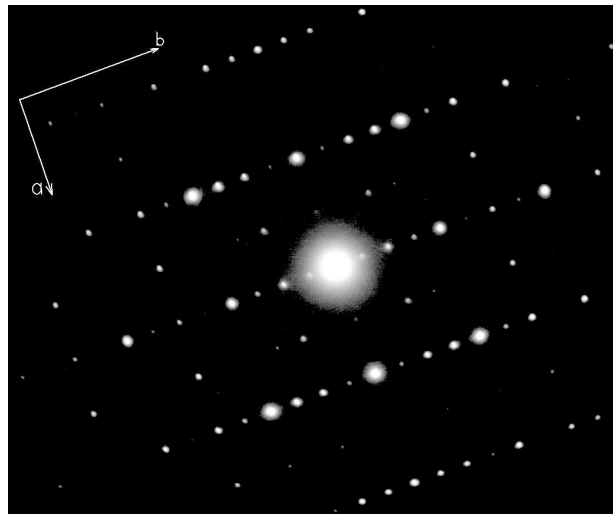


FIG. 5: Electron diffraction of (Mn,W)-DA6, showing the  $ab$  plane.

Hybrid material	Inorganic			Organic			I:O Ratio
	M	W	O	C	H	N	
(Mn,W)-DA2	1.059	0.941	3.883	2	10.44	1.84	1:0.40
(Mn,W)-DA6	1.129	0.871	3.742	6	17.3	1.89	1:0.39
(Mn,W)-DA8	1.226	0.774	3.549	8	19.41	1.85	1:0.54
(Mn,W)-DA12	0.897	1.103	4.205	12	27.58	1.93	1:0.53

TABLE I: Elemental analysis results for transition metal hybrids, showing the inorganic results calculated from EDX analysis, organic results calculated from elemental microanalysis, and the inorganic:organic (I:O) ratio. Calculated for  $M + W = 2$ ,  $C$  = number of carbon atoms in the alkyl chain.

W and Mn valences of 6+ and 2+ respectively. Combined with the EDX analysis, the inorganic layer has the formula  $[\text{Mn}^{2+}\text{W}^{6+}\text{O}_4]^0$ . As a result, the amine terminations of the organic molecules are also neutral (as already indicated in the IR spectra by the absence of any  $-\text{NH}_3^+$  modes). In contrast, the pure tungsten hybrids consist of  $\text{WO}_4^{2-}$  monolayers which must be balanced by charged diammoniumalkane  $[\text{H}_3\text{N}(\text{CH}_2)_n\text{NH}_3]^{2+}$  species [25].

Like the IR spectra indicating the structural similarity of the inorganic layer in each of the hybrids, the EXAFS spectra also appear virtually identical for the three compounds studied ( $\text{MnWO}_4 \cdot n\text{H}_2\text{O}$ , (Mn,W)-DA2 and (Mn,W)-DA6).  $\text{MnWO}_4$  was used as a starting model, and the final fitted results are given in Table II. The co-ordination numbers are quite uncertain past the third (W-W) shell. This is most likely due to the presence of several shells in this region, to which fits were also attempted without success.  $\text{MnWO}_4$  gives the following shells: W-W 3.281 Å, W-O 3.359 Å, W-Mn 3.521 Å, W-Mn 3.582 Å, W-O 3.602 Å. It is possible then that the W-W and W-O shells reported in Table II have much higher co-ordination numbers than in the actual system,

Shell	Length ( $\text{\AA}$ )	Co-ordination number
W-O	$1.737 \pm 0.021$	$2.11 \pm 0.64$
W-O	$2.121 \pm 0.022$	$4.82 \pm 1.39$
W-W	$3.233 \pm 0.024$	$6.63 \pm 3.58$
W-O	$3.337 \pm 0.033$	$12.21 \pm 3.61$
Mn-O	$2.124 \pm 0.007$	$4.76 \pm 0.40$
Mn-Mn	$3.409 \pm 0.041$	$1.28 \pm 0.80$

TABLE II: Averaged EXAFS results from fitting analysis of manganese tungstate hybrids.

as the other W-Mn and W-O shells have not been included in the fit, but would contribute to the spectra in the same region. It is also important to remember that EXAFS gives an averaged result.

Two shorter W-O bonds ( $1.7 \text{\AA}$ ) and four longer ones ( $2.1 \text{\AA}$ ) are observed, which most likely correspond to the normally distorted  $\text{WO}_6$  octahedra. In  $\text{MnWO}_4$  the tungsten oxide octahedra are edge shared, and the W-W distance is consistent with both  $\text{W} \langle \text{O} \rangle \text{W}$  linked via the two longer W-O planar bonds, and for W-O-W linked via the shorter apical bond. The next W-O shell observed probably corresponds to the distance from one tungsten atom to the apical oxygen atoms of its neighboring octahedra.

Fitting to the manganese data was more difficult, indicating that the positions of the manganese atoms are more disordered than those of the tungsten. In  $\text{MnWO}_4$  the  $\text{MnO}_6$  octahedra are edge-shared to one another and corner-shared to the tungsten oxide octahedra they sit between [26, 27]. However, it appears in the hybrids that one of the oxygen atoms is missing from the  $\text{MnO}_6$  octahedra, forming a square-based pyramid. The next nearest atom is another manganese, and there are either one (i.e. Mn dimers) or two (1D chains). However, only these two shells were used in the fit and there may be other Mn-Mn bonds relatively close which would appear in subsequent shells (as well as other Mn-W and Mn-O neighbors).

Combining the results presented so far, Figure 6 shows the proposed structure for the inorganic layer. Here the organic molecules are positioned in a row above the  $\text{MnO}_5$  square pyramids only and not above the  $\text{WO}_6$  octahedra. There are therefore two metal cations (W + Mn) to every organic molecule, consistent with the elemental analysis. Bond-valence sums [28, 29] for this structure, with bond lengths taken from the EXAFS data, yield valences of  $V_{\text{Mn}} = 2.03 \pm 0.03$  and  $V_{\text{W}} = 5.56 \pm 0.33$  which are in good agreement with the values obtained from the XANES results. From this the manganese is determined to have  $S = \frac{5}{2}$  and tungsten has  $S = 0$ . Thus any magnetism observed is due solely to the arrangement and interaction of the manganese atoms.

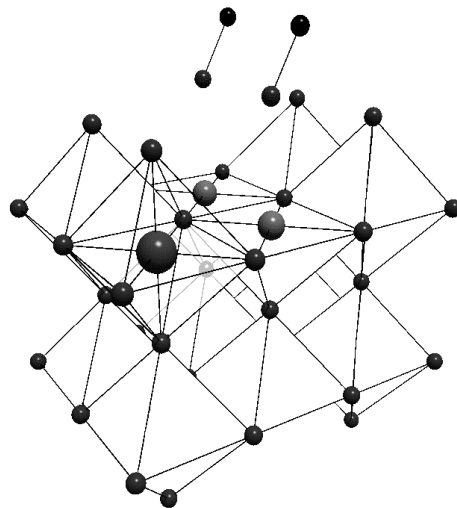


FIG. 6: Proposed structure of the inorganic layer of (Mn,W)-DAn hybrids. The nitrogen and first carbon atom of the organic molecules are shown. Small spheres = oxygen, middle spheres = manganese, large spheres = tungsten.

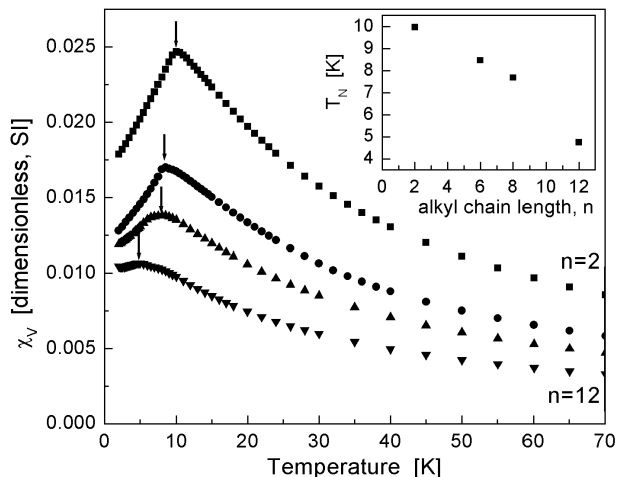


FIG. 7: DC susceptibility of (Mn,W)-DAn series ( $n = 2, 6, 8, 12$  from top to bottom).  $T_N$  is indicated by the arrows and plotted in the insert versus alkyl chain length.

## MAGNETIZATION STUDY

The DC susceptibility of a series of (Mn,W)-DAn hybrids is shown in Figure 7. The field- and zero-field-cooled curves are identical, indicating that the magnetization is reversible. There is no field-dependence of the susceptibility ( $\propto M/H$ ) for applied fields up to 1 T.

In each case there is a transition at low temperatures, indicated by the arrows. For (Mn,W)-DA2 and (Mn,W)-DA6 especially, the feature is cusp-like, characteristic of an antiferromagnetic (AF) ordering transition. (The clarity of the transition in these two samples is probably related to their increased crystallinity compared with the longer chain alkane hybrids.)

The Néel temperature is plotted as a function of alkyl chain length in the insert of Figure 7. This shows a monotonic decrease in  $T_N$  as the alkyl length, and hence the interlayer spacing, increases. It is expected that as the interlayer spacing is increased the interlayer coupling will decrease, which in turn will cause the transition temperature to decrease. This is qualitatively what is observed.

Curie-Weiss fits to the high-temperature parts of the curves ( $T > 50\text{K}$ ) display consistent Weiss temperatures: (Mn,W)-DA2:  $-19.6\text{K}$ , (Mn,W)-DA6:  $-19.6\text{K}$ , (Mn,W)-DA8:  $-19.9\text{K}$ , (Mn,W)-DA12:  $-20.1\text{K}$ . This is in contrast with the ‘parent’  $\text{MnWO}_4$  compound which has a Weiss temperature of  $-72\text{K}$  [30]. This parent compound is not layered and hence exhibits stronger AF ordering in 3 dimensions [27], which is weakened in the case of the layered hybrid materials.

From the proposed structure in Figure 6, as determined from TEM, EXAFS, and XRD, the arrangement of the manganese ions resembles that of a spin ladder compound. However, no empirical or theoretical model yet exists for  $S > \frac{1}{2}$  and in the few literature examples of spin ladder compounds with  $S > \frac{1}{2}$ , comparisons are made between the observed magnetization and models for chains and dimers [12, 13]. The (Mn,W)-DA2 DC susceptibility is shown in Figure 8 to a model for antiferromagnetic Heisenberg  $S = \frac{5}{2}$  chains [31, 32], given by

$$\chi = \frac{C}{T - \Theta} \left( \frac{1 - u}{1 + u} \right) + TIP,$$

$$u = \frac{T}{T_0} - \coth \frac{T_0}{T}, \quad T_0 = \frac{2JS(S+1)}{k_B}$$

This model resembles the Curie-Weiss law, with an additional temperature-dependent perturbation, where  $J$  is the coupling within the chains and  $S = \frac{5}{2}$  is the spin of the ion. (This is the limit of the spin ladder as  $J_{\perp} \rightarrow 0$ .) The chi-squared degree of fit for the AF chain model indicates a better fit than the simple Curie-Weiss, and matches the curve almost up to the AF transition (as shown in the insert).

From the fit parameters, the intrachain coupling value,  $J$ , has a value of  $J/k_B = -1.20\text{K}$ . This is comparable with similar values obtained for layered manganese phosphate hybrids of  $-0.79\text{K}$  [33] and  $-1.66\text{K}$  [34].

## COPPER ANALOGUE

If a compound with the same structure as Figure 6 could be formed with copper instead of manganese, this would represent a new variety of copper oxide  $S = \frac{1}{2}$  spin ladder, with the potential for doping in order to obtain new properties.

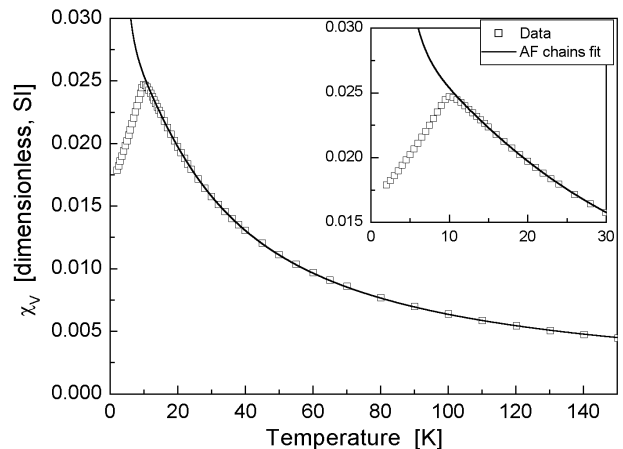


FIG. 8: DC susceptibility of (Mn,W)-DA2 with best fit curve to the Heisenberg AF chain model (fitted to  $T > T_N$ ).

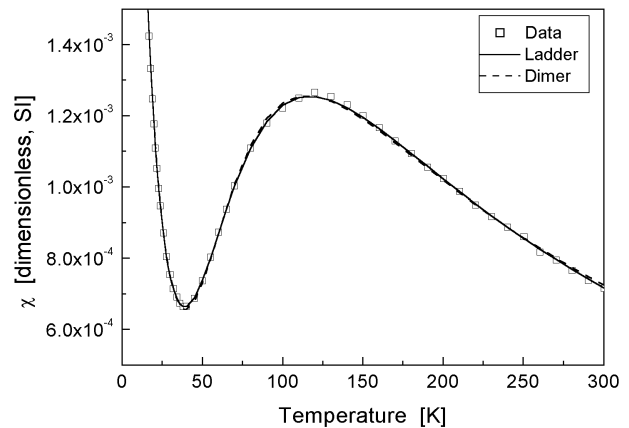


FIG. 9: DC susceptibility of (Cu,W)-DA6 with best fit curves for the spin dimer and spin ladder models.

A copper tungstate-DA6 hybrid has been synthesized, however like the manganese sample, full structural analysis has not been possible because of the small crystallite sizes. Despite this, there is reason to believe it may form a related structure, as its magnetization curves strongly resemble those observed in other spin- $\frac{1}{2}$  ladder systems. Figure 9 shows the DC susceptibility of (Cu,W)-DA6. There is no irreversibility and the susceptibility is independent of field.

A dimer model (Equation 1) suggested in Ref. [35] is as follows:

$$\chi = \frac{2Ng^2\mu_B^2}{3k_B T} \left[ 1 + \frac{1}{3} \exp(-2J/k_B T) \right]^{-1} + \frac{C}{T - \Theta} + TIP \quad (1)$$

It fits the (Cu,W)-DA6 data extremely well, with the following fit parameters:  $g = 0.413 \pm 0.001$ ;  $J/k_B = -102.9 \pm 0.2\text{K}$ ;  $C = 0.0277 \pm 0.0003\text{K}$ ;  $\Theta = 0.17 \pm 0.08\text{K}$ ;  $TIP = -0.00022 \pm 0.000007$  ( $\chi^2/DoF = 4.437 \times 10^{-11}$ ).

A spin ladder model for  $S = \frac{1}{2}$  was also fitted to the

data. Due to the good agreement between the spin dimer model and the experimental data, we assume that in the spin ladder model  $J_{\perp} \gg J_{\parallel}$  and all other exchanges ( $J_{diag}$ ,  $J_{interchain}$ , etc.) are negligible. We used the fit in Ref. [7] for isolated chains with  $J_{\perp}/J_{\parallel} \geq 1$ :

$$\begin{aligned} \chi(T) &= \frac{N_A g^2 \mu_B^2}{J_{\perp}} \chi^*(t) + \frac{C}{T - \Theta} + TIP; \\ \chi^*(t) &= \frac{\exp(-\Delta_{fit}^*/t)}{4t} \mathcal{P}_q^p(t); \\ t &\equiv \frac{k_B T}{J_{\perp}}, \\ \mathcal{P}_q^p(t) &= \frac{1 + \sum_{n=1}^p N_n/t^n}{1 + \sum_{n=1}^q D_n/t^n} \end{aligned} \quad (2)$$

where the parameters  $\Delta_{fit}^*$ ,  $N_n$  and  $D_n$  (all functions of  $J_{\parallel}/J_{\perp}$ ) are given in Appendix 5 of Ref. [7].

The following fitted parameters were obtained:

$g = 1.920 \pm 0.008$ ;  $J_{\parallel}/k_B = -0.3 \pm 1.4\text{K}$ ;  $J_{\perp}/k_B = 213.6 \pm 1.1\text{K}$ ;  $C = 0.0268 \pm 0.0003\text{K}$ ;  $\Theta = -0.0015 \pm 0.0004\text{K}$ ;  $TIP = -0.0003 \pm 0.00001$  ( $\chi^2/DoF = 2.3718 \times 10^{-11}$ ).

The two fits are compared in Figure 9 with the experimental data. The ladder model is shown as the solid line and the dimer model as the dotted line. Comparing the two fits, we note firstly that the assumption  $J_{\perp} \gg J_{\parallel}$  is valid and therefore the spin dimer model should be sufficient to describe the (Cu,W)-DA6 system. However, the spin dimer model does not give an accurate  $g$  factor - the expected value is  $\sim 2$ , whereas the dimer model yields  $g = 0.413$ . However the spin ladder model gives  $g = 1.920$ , in good agreement with the expected value and consistent with other  $\text{Cu}^{2+}$   $S = \frac{1}{2}$  systems [35]. The exchange constant  $J_{\perp}$  between the two Cu atoms of the dimer in the ladder model is roughly double that obtained for the dimer model; this is due to a difference of notation in the two models. (In the exponential term of the dimer model (Equation 1), one has a factor of 2 that is not present in the exponential term of the spin ladder fit (Equation 2)). The values of  $C$  and  $TIP$  are virtually identical. While  $\Theta$  has different signs in each of the two models, it has a small value so can be essentially treated as zero.

## CONCLUSIONS

Indirect methods of structural analysis of a manganese tungstate diaminoalkane hybrid series strongly suggest that this compound forms a spin ladder-type structure with  $S = \frac{5}{2}$ . Magnetization results indicate that the system behaves like a 1D AF Heisenberg chain, so it is likely that  $J_{\parallel} \gg J_{\perp}$ . A copper tungstate hybrid on the other hand fits well to a spin ladder model with  $J_{\perp} \gg J_{\parallel}$ , thus behaving more like a spin dimer system. The fact

that the spin ladder model gives a more reasonable value of  $g$ , and has a better  $\chi^2/DoF$  value than the dimer model, indicates that the spin ladder model probably has some validity.

Future work in this area includes attempts to dope the inorganic layer through electrochemical means. It should also be possible to form samples with composition  $\text{Mn}_{1-x}\text{Cu}_x\text{WO}_4$ -DAn to determine the structure and magnetism across the solid-solubility series.

## ACKNOWLEDGEMENTS

The authors would like to acknowledge the financial assistance from the New Zealand Foundation of Research Science and Technology (Contract number: IRLX0201), The Royal Society of New Zealand Marsden Fund, and the MacDiarmid Institute for Advanced Materials and Nanotechnology (Victoria University, New Zealand).

- 
- [1] Z. Hiroi, M. Azuma, M. Takano, and Y. Bando, *J. Solid State Chem.* **95**, 230 (1991).
  - [2] T. Barnes and J. Riera, *Phys. Rev. B* **50**, 6817 (1994).
  - [3] E. Dagotto, J. Riera, and D. Scalapino, *Phys. Rev. B* **45**, 5744 (1992).
  - [4] E. Dagotto, *Rep. Prog. Phys.* **62**, 1525 (1999).
  - [5] E. Dagotto and T. M. Rice, *Science* **271**, 618 (1996).
  - [6] M. Uehara, T. Nagata, J. Akimitsu, H. Takahashi, N. Mori, and K. Kinoshita, *J. Phys. Soc. Japan* **65**, 2764 (1996).
  - [7] D. C. Johnston, M. Troyer, S. Miyahara, D. Lidsky, K. Ueda, M. Azuma, Z. Hiroi, M. Takano, M. Isobe, Y. Ueda, et al., *cond-mat/0001147* (2000).
  - [8] M. Onoda and N. Nishiguci, *J. Solid State Chem.* **127**, 359 (1996).
  - [9] D. C. Johnston, J. W. Johnston, D. P. Goshorn, and A. J. Jacobson, *Phys. Rev. B* **35**, 219 (1987).
  - [10] B. C. Watson, V. N. Kotov, M. W. Meisel, D. W. Hall, G. E. Granroth, W. T. Montfooj, S. E. Nagler, D. A. Jensen, R. Backov, M. A. Petruska, et al., *Phys. Rev. Lett.* **86**, 5168 (2001).
  - [11] R. D. Willett, C. Galerii, C. P. Landee, M. M. Turnbull, and B. Twamley, *Inorg. Chem.* **43**, 3804 (2004).
  - [12] D. J. Price, A. K. Powell, and P. T. Wood, *J. Chem. Soc., Dalton Trans.* p. 3566 (2000).
  - [13] D. J. Price, A. K. Powell, and P. T. Wood, *J. Chem. Soc., Dalton Trans.* p. 2478 (2003).
  - [14] J. Kreitlow, D. Baabe, A. U. B. Wolter, S. Süllow, F. J. Litterst, D. J. Price, and H. H. Klaus, *J. Magn. Magn. Mater.* **272**, 152 (2004).
  - [15] T. Sakai, N. Okazaki, K. Okamoto, K. Kinodo, Y. Narumi, Y. Hosokoshi, K. Katoh, K. Inoue, and T. Goto, *Physica B* **329**, 1203 (2003).
  - [16] K. Katoh, Y. Hosokoshi, K. Inoue, M. I. Batashevich, H. Nakano, and T. Goto, *J. Phys. Chem. Solids* **63**, 1277 (2002).
  - [17] S. V. Chong, B. Ingham, and J. L. Tallon, *Curr. Appl. Phys.* **4**, 197 (2004).

- [18] B. Ingham, S. V. Chong, and J. L. Tallon, *Mat. Res. Soc. Symp. Proc.* **775**, 165 (2003).
- [19] B. Ingham, S. V. Chong, and J. L. Tallon, *Curr. Appl. Phys.* **4**, 202 (2004).
- [20] B. Ingham, S. V. Chong, and J. L. Tallon, *Mat. Res. Soc. Symp. Proc.* **847**, EE9.31 (2005).
- [21] J. H. Choy, Y. S. Han, N. G. Park, H. Kim, and S. W. Kim, *Synth. Met.* **71**, 2053 (1995).
- [22] Y. Tsunoda, W. Sugimoto, and Y. Sugahara, *Chem. Mater.* **15**, 632 (2003).
- [23] Z. Liu, K. Ooi, H. Kanoh, W. Tang, and T. Tomida, *Langmuir* **16**, 4154 (2000).
- [24] M. Kudo, H. Ohkawa, W. Sugimoto, N. Kumada, Z. Liu, O. Terasaki, and Y. Sugahara, *Inorg. Chem.* **42**, 4479 (2003).
- [25] B. Ingham, S. V. Chong, and J. L. Tallon, *J. Phys. Chem. B* **109**, 4396 (2005).
- [26] R. O. Keeling Jr., *Acta Cryst.* **10**, 209 (1957).
- [27] G. Lautenschläger, H. Weitzel, T. Vogt, R. Hock, A. Boehm, M. Bonnet, and H. Füss, *Phys. Rev. B* **48**, 6087 (1993).
- [28] D. Altermatt and I. D. Brown, *Acta Cryst. B* **41**, 240 (1985).
- [29] I. D. Brown and D. Altermatt, *Acta Cryst. B* **41**, 244 (1985).
- [30] L. G. van Uittert, R. C. Sherwood, H. J. Williams, J. J. Rubin, and W. A. Bonner, *J. Phys. Chem. Solids* **25**, 1447 (1964).
- [31] R. Dingle, M. E. Lines, and S. L. Holt, *Phys. Rev.* **187**, 643 (1969).
- [32] M. E. Fisher, *Am. J. Phys.* **32**, 343 (1964).
- [33] Z. A. D. Lethbridge, M. J. Smith, S. K. Tiwary, A. Harrison, and P. Lightfoot, *Inorg. Chem.* **43**, 11 (2004).
- [34] Y. Song, P. Y. Zavalij, N. A. Chernova, and M. S. Whittingham, *Chem. Mater.* **15**, 4968 (2003).
- [35] R. S. Rarig Jr., R. Lam, P. Zavalij, J. K. Ngala, R. L. LaDuca Jr., J. E. Greedan, and J. Zubieta, *Inorg. Chem.* **41**, 2124 (2002).